Published in final edited form as:

Nano Res. 2018 September ; 11(9): 4549–4561. doi:10.1007/s12274-018-2035-7.

DNA-Encoded Morphological Evolution of Bimetallic Pd@Au Core-shell Nanoparticles from a High-indexed Core.

Nitya Sai Reddy Satyavolu[†], **Nikou Pishevaresfahani**[†], **Li Huey Tan**[†], and **Yi Lu**[†]

[†]The Department of Chemistry, University of Illinois at Urbana-Champaign, Urbana, Illinois 61801, United States.

Abstract

DNA-mediated synthesis of nanoparticles with different morphologies has proven to be a powerful method to synthesize and access many exclusive shapes and surface properties. While previous studies employ seeds that contain relatively low-energy facets, such as a simple cubic palladium seed in the synthesis of Pd-Au bimetallic nanoparticles, few studies have investigated whether DNA molecules can still exert their influence when the synthesis uses a seed that contains high-energy facets. Seeds that are enclosed by such high-energy facets or sites are known to act as easy nucleation sites in nanoparticles growth and could potentially suppress the effect of DNA. To answer this question, we herein report DNA-encoded control of morphological evolution of bimetallic Pd@Au core-shell nanoparticles from a concave palladium nanocube seed that contains high indexed facets. Based on detailed spectroscopic and SEM studies of time-dependent growth of the bimetallic nanoparticles, we found that each of 10-mer DNA molecules (T10, G10, C10 and A10) has a unique way of interacting with both the seed's surface and the precursor. Among them, the most important factor is the binding affinity of the nucleobase to the Pd surface, with the A10 possessing the highest binding affinity and thus capable of stabilizing the seed's high energy surfaces. Furthermore, for bases with lower binding affinity (T10, G10 and C10) than A10, the growth is completely dictated by the seed's surface energy initially, but the later growth can still be influenced by the different DNA sequences, resulting in four unique morphologically different Pd@Au bimetallic nanoparticles. The effect of these DNA molecules with medium binding affinity can only be observed when there is more deposition of Au. Based on the above results, a scheme for the DNA controlled growth is proposed. Together these results have provided insights into factors governing DNA-mediated growth of core-shell structures using seeds with high-energy sites, and the insights can readily be applied to other bimetallic systems that adopt seed-mediated synthesis.

GRAPHICAL ABSTRACT

Address correspondence to Yi Lu, yi-lu@illinois.edu.

Electronic Supplementary Material: Supplementary material (Additional notes on fitting of kinetic data, absorption studies, characterization of seed and particles, SERS studies and additional supporting figures of SEM and TEM images have been included) is available in the online version of this article at http://dx.doi.org/10.1007/s12274-***-****-* (automatically inserted by the publisher).

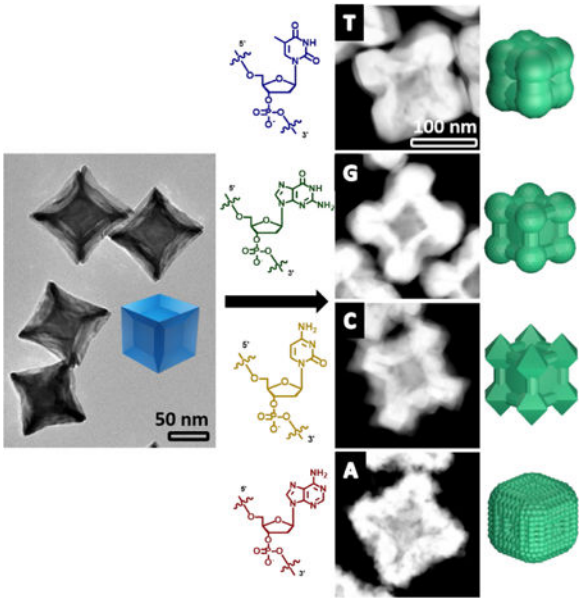

This paper reports DNA encoded growth of morphologically unique gold shells on a high-indexed palladium seed and mechanistic study on how DNA base affinity plays an important role in overriding the effect of high-energy facets of the core and in the formation of Pd@Au bimetallic core-shell nanostructures.

Keywords

Concave seed; DNA; shape-control; Pd@Au core-shell nanoparticles

1 Introduction

The synthesis of metal nanoparticles with different shapes and surface properties has been a major focus of research [1–4], as the resulting morphologies play a major role for applications in areas such as optics [5–10], catalysis [11–16], sensing [8, 17–20], imaging [21–25], and biomedicine [24, 26–33]. To control the morphologies of metal nanoparticles, most researchers employ different capping ligands, such as Cetyl Trimethyl Ammonium Bromide (CTAB), Polyvinylpyrrolidone (PVP) or halides [34] as a key strategy [35]. These ligands play a significant part in providing colloidal stability as well as stabilizing specific facets of the final nanoparticles. Recognizing that DNA can be a special programmable ligand in assembly [3, 36–42] and nanoparticle synthesis, we and others have demonstrated that DNA can control morphologies of many metal nanoparticles with exceptional precision, and the resulting morphologies are highly dependent on different DNA sequences used [43–49]. This unique DNA-encoded approach to controlling nanoparticle morphologies stems from sequence-specific interactions of the DNA with metal surfaces. For example, we have recently reported the DNA mediated growth of bimetallic nanoparticle where a seed mediated co-reduction of palladium and gold onto a cubic palladium core was involved [48]. The seed was characterized by {100} facets and additional {110} and {111} sites constituting the edges and corners respectively. The presence of DNA specifically

contributed to the nucleobase binding to the low co-ordination sites on the seed, i.e., the {110} and the {111} sites. The affinity of the different DNA sequences to these sites as well as to the metal precursors in the reaction environment play a key role in determining the mechanism of initial metal deposition and diffusion onto the seed.

While the above studies have established that DNA can play a major role in controlling the morphologies of different nanoparticles, all the studies reported so far involve seeds that contain low-indexed facets with exceptions of twinned surfaces; the presence of low-indexed facets made it possible for the DNA to bind to the metal surface of the seeds and influence the shell growth on the seed from the very initial phase. We wondered if DNA molecules with different sequences can still exert their influence on the surface of seeds that contain higher-energy sites, and if yes, what factors are crucial in doing so. Answering these questions will provide much deeper insight into the roles of the ligand in fine-tuning morphologies of nanoparticles and expand the methodology of DNA-encoded nanoparticle growth to synthesize a wide variety of nanomaterials with diverse morphologies. To provide answers to the above questions and gain deeper insight into the mechanism of morphological control of bimetallic nanoparticles, we report herein DNA-mediated synthesis of nanoparticles, with a concave palladium cube seed of ~75 nm as the core. When compared to a simple palladium nanocube, the as-synthesized concave cube has protruding edges and corners, presenting metal atoms that are highly unsaturated with respect to coordination. By adopting the concave cube, we intended to test specifically if the presence of higher energy facets suppresses the effect of DNA in controlling the morphology of the final nanomaterials. We found that DNA molecules can still exert their influence on morphologies of the nanomaterials and the effects of different DNA sequences are different from those observed in the synthesis where a simple palladium nanocube is used as a seed. A new scheme for the DNA controlled growth in presence of high-energy sites is proposed.

2 Experimental Section

2.1 Synthesis of ~22 nm Cubic Pd NC Substrates:

PdNCs were synthesized by following a previously reported protocol [50]. Diluted HCl is added to $PdCl_2$ (in 2:1 ratio) to produce a 10 mM H_2PdCl_4 solution. Briefly, a vial containing CTAB (45.6 mg) and 10 mL of deionized water was sonicated until the CTAB was completely dissolved. Pd precursor (0.500 mL of 0.01 M H_2PdCl_4) was added to the solution, and a bright orange color was produced indicating the formation of the precursor complex with CTAB. The solution was then heated for 5 min at 95 °C with stirring (~600 rpm), after which 0.080 mL of 0.1 M ascorbic acid was added to the vial. The solution was left to heat for an additional 15–20 min at 95 °C with stirring to form a clear brown colored solution indicating the formation of the NC substrates. The solution was removed from heat and stored at 30 °C.

2.2 Synthesis of Pd Concave Cube substrates:

Pd NCs were synthesized by following a previously reported protocol with modifications [51]. Briefly, CTAB (182.24 mg) was dissolved in 5 mL of Millipore water and transferred to a 15 mL tube. To this solution, 100 μL of 1 mM $CuSO_4$ solution was added and mixed

gently. This solution was placed in a water bath maintained at 40 °C. To this solution, H_2PdCl_4 (0.125 mL of 0.01 M H_2PdCl_4) was added and mixed. The previously prepared 22 nm Pd cube seed solution (75 μL) was then added to the above solution and mixed. Finally, ascorbic acid (150 μL, 0.1 M) was then added to the solution and the reaction contents were mixed gently and then kept at 40 °C. The reaction was left to remain still for 12 h until the reaction was complete. Typically, a blue colored solution shall result at the end of the reaction. These particles were then used for the DNA-mediated synthesis.

2.3 DNA-Mediated Synthesis of Pd@Au Bimetallic Nanocrystals:

Typically, the concave cube solution was first washed close to 3 times by centrifugation (8 krpm for 5 min) to remove the existing CTAB as much as possible. The washed solution was then diluted to have an absorbance of 0.3 at around 700 nm (concentration ~4.8 ppm Pd as determined by ICP-MS). Then, 100 μL of the diluted solution were incubated in oligomeric sequences of DNA for around 15 min (A10, T10, G10, and C10). 1 μL of ~1 mM DNA stock solutions were added to the absorbance adjusted particles. 200 mM $NH_2OH{\cdot}HCl$ solution was adjusted to pH 5 by using a conc. solution of NaOH. 0.6 μL of this pH adjusted solution was then added to the DNA incubated cubes and then 2 μL or 6 μL of 5 mM $HAuCl_4$ was added depending upon whether a low or high concentration of precursor is being used for the study, respectively. The reaction was then left to completion. Kinetic absorption studies: The change in the absorption spectra of the nanoparticles during the growth was monitored by performing the experiments in a quartz cuvette itself. The working volumes for all the samples were kept the same as when the nanoparticle growth was performed in an Eppendorf tube.

2.3 Kinetic SEM studies:

In order to arrest the growth of a sample at a certain time point, 1 μL of 3-mercaptopropanoic acid (100 mM, MPA) was added to the solution along with 10 μL of 0.2% SDS. The sample was then subjected to centrifugation and washed with Millipore water 3 times before characterizing using SEM or TEM.

3 Results and Discussion

The concave palladium seeds were synthesized using a slightly modified protocol reported by Niu et. al [51] to form a light blue colored solution (Fig 1a, Fig S2 in the ESM). The absorption spectrum of this blue colloidal solution exhibited a broad peak in the near infrared (NIR) range with the absorbance maximum at ~730 nm (Fig S3). This seed is enclosed by protruding edges in the <110> and the <111> directions, but retains the six {100} facets on the core, as indicated by the SAED pattern in Fig 1c. The extended edges and tips on the concave nanocube are energetically unstable, due to the smaller number of neighboring atoms as compared to those in a simple nanocube [52]. This property becomes evident when the nanoparticle is aged, as the smoothening of the edges is observed with time (Fig. S4), accompanied by change in the color of the solution to brownish-orange.

Gold precursor was reduced by hydroxyl amine and then deposited onto the palladium concave cubic seed in the presence of DNA molecules, each of which contains repeating

units of 10 nucleobases (referred to as T10, G10, C10 and A10 hereafter). We have previously demonstrated that the morphology control of nanoparticles is independent of the length of the DNA sequences, but a DNA sequence that is too short (e.g., 5 bases) cannot provide enough colloidal stability [44, 46]. Therefore, strands consisting of 10 bases or longer have been typically used in our studies, but beyond a certain length that maintains such stability, the length of the DNA plays little role. Additionally, since we used 10 bases for our previous study with the simple cubic seed, we continued to use the same sequences for our concave system for a direct comparison. All the reactions were performed at room temperature and in water. The reduction of $HAuC_4$ was performed and the resultant morphologies in the presence of T10, G10, C10 and A10 were studied. The results obtained were indeed sequence dependent as observed by the SEM images (Fig. 1). The presence of T10 caused the formation of a gold shell with less deposition of gold along the {100} facet and more deposition in the <111> and <110> directions. The process of gold deposition in the presence of G10 and C10 was similar in that there was more visible deposition along the <111> direction. However, G10 has vertices that are rounded off while C10's edges form octapods, with octahedron-like structures consisting of prominent {111} surfaces. Finally, A10 resulted in formation of a gold shell on the palladium seed with an overall rough surface. The formation of such unique structures from the same core often require careful and articulate tailoring of a variety of different conditions and reagents [53]. In contrast, in the presence of different sequences of DNA, these different morphologies can be formed reproducibly in quantitative yield under the same condition.

To confirm the elemental composition of the core-shell structures observed in Fig. 1, the nanoparticles were analyzed by STEM-EDS (Fig. 2), which confirmed the presence of palladium in the core and gold in the shell. Interestingly, these images reveal that, for all the core-shell structures formed under this condition, the gold shell formed on the {100} facet of the Pd core (which is the lower surface energy (γ) facet) is thinner than the gold shell deposited onto the edges and vertices of the Pd core (which are the higher γ sites). The extent of the shell thickness varies depending on the DNA sequence. For example, the growth in presence of T10, G10 and C10 bases shows a very prominent crater like feature in the <100> directions, similar to those observed in the seed). On the other hand, this feature is less prominent along the {100} facets in the presence of A10. The absorption spectra of all the particles had λ_{max} values beyond 700 nm and in the NIR range (Fig. S5). Given the unique architecture and absorption spectra of the core-shell structures, we predicted that they can be used for Surface Enhanced Raman Spectroscopy (SERS). The structures did indeed show enhancement factors of the order of 107 in the spectra of 4-mercaptobenzenethiol (4-MBT, see Fig. S6 & SI SERS Properties of the DNA mediated Pd@Au Nanoparticles).

3.1 Kinetic study of DNA-mediated growth of Pd@Au core-shell nanoparticles:

Given the different core-shell structures observed in the presence of different DNA sequences in Figures 1 and 2, we investigated the kinetics of the gold shell formation via absorption spectroscopy where absorption changes associated with the gold shell growth were monitored in-situ. Since it is established that the absorbance of the surface plasmon peak is directly related to the volume fraction of the nanoparticles grown as a function of time, absorption spectroscopy can provide us with useful information about the evolution of

the nanoparticle structure [54]. The growth of Au shell on the Pd concave cube seed showed an increase in the absorbance in the NIR region involving continuous shifts in λ_{max} wavelengths, initially a red shift, followed by a blue shift, in the presence of all DNA sequences (Fig. 3a). These shifts in the wavelengths can be attributed to the coupling of the Surface Plasmon Resonance (SPR) of Pd concave cube (λ_{max} = 730 nm) with that of the Au shell, resulting in the final particles having an SPR in the NIR region. In our previous system where the simple palladium cube (SPR ~400 nm) was used as the seed, the emergence of the plasmonic peak (due to the gold deposition) was observed but did not exhibit any plasmonic coupling and hence no shift in the λ_{max} with time was observed. Notably, in the current concave system, the extent of red shift was the least for the T10-mediated particles (final λ_{max} = 820 nm) and the most for the A10-mediated nanoparticles (final λ_{max} = 862 nm), with the G10 and C10 particles (λ_{max} = 836 nm and 847 nm, respectively) in between (Fig. S5).

In addition to the main SPR peak in the NIR region, a shoulder peak ~550 nm is present in the as-synthesized nanoparticle structures, indicating the inherent anisotropicity of the core-shell particles [7]. The shoulder peak is less prominent for the A10-mediated particles as compared to the spectral profiles of the particles synthesized with T10, G10 and C10, which is in good agreement with the absence of the prominent crater like feature along the <100> direction in the A10 mediated particles. To better analyze the kinetic growth profiles, the absorbance values at the final λ_{max} in the NIR region were plotted against time (Fig. 3b). Since the absorbance of the particles is sensitive to the morphology at a given time, the extinction coefficient changes as the particles grow in solution. The plots of absorbance at λ_{max} against time revealed an exponential growth curve in the presence of T10, G10 and C10, but a sigmoidal growth curve in the presence of A10. Considering that the system involved plasmonic coupling between the Pd core and the Au shell that resulted in the continuous shift of the λ_{max} peak during the growth, we integrated the area under the curves between 500 nm to 1000 nm and plotted against time (Fig. 3b). The profiles showed the same trend, corroborating our initial analysis of time trace of absorbance at λ_{max}. The rate of increase in absorbance was the highest in the case of T10-mediated growth and lowest in the case of A10-mediated growth. The growth curves started to level off at ~ 25 min into the growth process, even though the same amount of reductant was used [48]. In comparison, the growth process for the simple cubic system took more than 1 hr to reach completion. The faster rate in the current concave seed system can be attributed to the higher precursor (Au) concentration and the high-γ sites on the current seed. The curves were fit by adopting the widely used KJMA (Kolmogorov-Johnson-Mehl- Avrami) model [54–57] (Fig. S7), which helped obtain kinetic parameters for the growth in the presence of all the bases (see Table S2 in the ESM for additional information on absorption kinetic data). For the bases that direct the exponential growth mechanism, the order of rate of increase in absorbance observed was T10>G10>C10. A10 showed a sigmoidal curve, indicating the aggregative growth mechanism [58, 59]. No change in absorbance was observed in the first 3–4 min, probably due to the formation of smaller nanocrystallites stabilized by A10, as a result of Ostwald ripening before depositing onto the concave seeds.

To be able to correlate the morphology to the absorption spectral changes, we then obtained time-dependent SEM images of these nanoparticles by arresting the growth of the

nanoparticles at different stages. The morphological evolution was studied by quenching the reaction at different time points with excess mercaptopropanoic acid (MPA), which is known to bind to the gold precursor and prevent further metal precursor reduction and hence deposition onto the seed [60]. On analyzing the images of the initial time points of the Au deposition on the Pd concave cube, the nucleation events on the Pd concave cube were very similar in the presence of different DNA sequences (Fig. 4). The formation of small Au islands on the Pd core is also similar in the presence of all the four bases, but the deposition profiles after the Au island formation are markedly different between the particles grown in the presence of A10 and those in presence of T10, G10 and C10. Specifically, the Au deposition is high along the <111> and the <110> directions and low along the <100> direction in the presence of T10, G10 and C10. The A10-mediated growth, on the other hand, shows an almost even Au deposition profile on all the facets of the concave Pd cube, explaining the absence of the deep crater along the <100> direction in the final particles. The intermediate particle morphologies in the presence of T10, G10 and C10 between 0–10 min look almost indistinguishable. Beyond the 14 min mark, distinct features of each morphology start to appear, including the rounding of vertices in the presence of G10 and the formation of the {111} surfaces in the presence of C10.

It is known that the surface energies of different facets of the concave cube are different, with the site protruding in the <111> direction having the highest energy, followed by the site protruding in the <110> direction, and then the site in the {100} facet with the lowest energy (Scheme 1). Regions on the surface of the seed that have uncoordinated atoms decreases the energy barrier for nucleation events [61, 62]. The difference in surface energies can be probed by growing the Au shell in the absence of any capping agent, as the growth of the shell would be mainly guided by surface energies. When the Pd seed alone was treated with just the Au precursor and the reductant, apart from the formation of aggregated nanoparticles due to the lack of a stabilizing agent, we noticed some separate particle clusters whose seed edges and corners were covered with a gold shell (Fig. S8). Among these separate clusters, the indentation along the <100> direction was observed, indicating that the area lacks Au deposition in this lowest surface energy direction (Fig. S8). Furthermore, the deposition along the <111> direction is almost always greater than the Au deposition along the <110> direction (Fig S8), implying that the γ is in the order of {100} < {110} < {111}. Therefore bases that have weak affinity towards the surface of the concave seed, would allow deposition in a way that is dictated by the surface energies of the seed. On the other hand, bases that have higher binding affinity will be able to bind to the surfaces of the seed thus resulting in the lowering of the surface energies and enabling the growth in a base-specific manner. Based on the time-dependent SEM study, we present a 2-D atomic model scheme, similar to the one proposed by Xia and coworkers [63], to describe the mechanism of the DNA-mediated Au nanoparticle deposition onto Pd concave seed (Scheme 1). In this 2-D atomic model, we chose the atomic plane that contains all the sites that participate in the growth, i.e., the plane cutting across the concave structure passing through two opposite protruding edges in the <110> direction, diagonally across two {100} facets and containing 4 corners protruding in the <111> direction.

T10 is known to have a low affinity to metal surfaces, due to the lack of functional groups in the thymine base that are capable of binding to metal atoms [64]. Therefore, this sequence

mostly contributes to the colloidal stability of the nanoparticles, and allows the deposition of metal atoms to take place in a way that is dictated by the surface energies of the Pd concave seed, as observed in the previous system [48]. While there is visible deposition along the {100} facet of the concave cube, the deposition is dominated on the edges and vertices. As deposition moves away from the center of the {100} facet to the edge, the amount of Au shell increases. The Au atoms deposited on the edges and corners are accommodated in sites around the {100} facet. In the STEM images (Fig. 2), the T10 mediated particles distinctly have higher deposition of Au on the edges and corners as compared to the nanoparticles mediated by the other DNA sequences. This deposition pattern is consistent with what we observed in the control sample that lacks a capping ligand (Fig. S8). The control, however, lacks colloidal stability, while the T10 helps provide that stability during the growth. In the kinetic study, the island like growth transitions into a smooth surface close to 7 min into the growth, with the deposition mostly along the <111> direction. The rate of deposition of Au atoms overpowers the rate of diffusion ($V_{deposition} >> V_{diffusion}$) and thus a thick shell is formed, mostly confined to the periphery (Scheme 1). When correlated to the kinetic absorption spectrum, the rough deposition of metal during the initial time points promotes a red shift of the λ_{max} value (close to 2 min due to an increased number of surface features) and the smoothening (beyond 4 mins) of the surface promotes a blue shift (Fig. 3a & S9) [65]. Beyond 7 min the emergence of secondary peak at 550 nm becomes clear indicating structural anisotropy.

When comparing the shape evolution mediated by T10 and G10, there is some amount of resemblance. The subtle difference between the two final shapes is the well-rounded corners formed in the presence of G10, which is essentially missing in the case of T10. The rounded corners of the shell mediated by G10 are separated by less deposition on the edges (<110> direction). The metal binding capability of G10 is higher than that of T10, via the carbonyl and the exocyclic amine group. Initial deposition on the seed can be observed on all sites of the concave seed, just like in T10. As time proceeds, the deposition in the <111> direction becomes more prominent due to γ effects, over the deposition on the edges protruding in the <110> direction, hence forming thicker rounded corners. Since the $V_{deposition} > V_{diffusion}$ the thickness of the shell along the {100} facet is the least (Scheme 1). Transition of the initial rough deposition to a smooth surface takes place after 10–14 min of the growth, and this transition can be observed even in the absorption spectra where the red to blue shift starts occurring around the 7^{th} min (Fig 3a & S10). Additionally, circular dichroism (CD) did not reveal any significant peak, indicating the absence of secondary structure formation by G10 in contrast to the previous cubic core system (Fig. S11). We hypothesized that the absence of Pd precursor may be a reason for the absence of secondary structure and we observed that the CD spectra with both Au and Pd precursor co-reduction showed a significant change in the CD feature (Fig. S11).

The presence of C10 forms octapod like structures. The chemical structure of the cytosine base also enables metal binding via functional groups such as amine. Similar to G10, the C10-mediated structures have lower thickness in the <110> direction and higher thickness in the <111> direction. Again, clearly the $V_{deposition} > V_{diffusion}$ rendering the formation of an asymmetric structure. The most interesting feature is the octahedral-like corners stabilized by the C10 sequence. The {111} facets are distinctly visible and are formed on all 8 corners

of the nanoparticle structure. The deposition along the <111> direction is the highest and the C10 sequence that exists in solution tends to stabilize the {111} facet, resulting in the formation of octahedral structures at these sites (Scheme 1). The process of {111} facet stabilization is evident close to the 14^{th} min in the kinetic stabilization study and the clear emergence of the secondary peak (Fig 3a & S12). The blue shift in the kinetic absorption spectra starts to occur at around 10 mins. This blue shift takes place later in the growth as compared to the growth in the presence of T10 and G10. We also noticed that some structures occasionally also show overgrowth along the <110> direction (Fig. S13), where there are octahedral like features along the edges, due to the overgrowth of the shell. The stabilization of the {111} surfaces by the C10 sequence is consistent with what we previously observed for Au deposition on either Au prism [47], Au nanorod [46], or Pd cubic seeds [48], where the final structures controlled by the cytosine containing sequence are enclosed by {111} facets.

Finally, In the presence of A10, there exists the dominance of aggregative growth mechanism which was also observed with the simple cubic core system [48] where the overall reaction rate was much slower. In the current system, the aggregative growth mechanism renders the least deposition within 2 min as compared to the other bases. This was also supported by the HR-TEM of the 2 min sample, which showed a number of smaller nano-crystallites around the seed (Fig. S14). The particles were washed a minimum of 3 times before subjecting to TEM analysis to avoid any precursor reduction in presence of the electron beam. It is clear that the deposition of the smaller nano-crystallites after Oswald's ripening is influenced by the surface energy (γ) of the concave seed's edges and vertices, i.e. the sites protruding in the <111> and <110> directions. The A10 oligonucleotide binds to these sites of high γ, as well as the precursor in the reaction solution, and thus lowers the corresponding γ of these sites. Therefore, the deposition takes place in the <111> and <110> directions and along the {100} facet. Even though the surface energy of the edges and the corners is lowered, the {100} facet still remains lower in energy, accounting for the formation of a slightly less thick shell in the <100> direction of the particle (Scheme 1). The rough surface of the nanoparticles, we hypothesize, can be due to two reasons; 1) since A10 binds to the precursor to form smaller nanoparticles, these nano-crystallites deposit on the seed's surface as is; 2) As observed in a previous system of gold deposition on gold seed in the presence of A30 [47], the rough surface is formed due to the low mobility of the adenine on the gold surface, thereby allowing the Au deposition to occur in areas that are devoid of the DNA strands. After the initial nucleation event of gold on the concave seed's surface, the A10 sequences in solution are able to interact with the deposited gold, essentially making it a gold on gold deposition thereafter. In the current system, the overall faster deposition rate of the small A10-stabilized nanocrystallites could contribute to the rough surface.

The kinetic studies have provided important information about the growth processes in the presence of the different DNA sequences. The $V_{deposition}$ is almost always greater than the $V_{diffusion}$ and this is largely dependent on the seed's surface energy and hence the growth is a highly deposition-dominated process. The extent to which $V_{deposition}$ is greater than $V_{diffusion}$ depends on the DNA sequence used. The nucleation kinetics are much faster if the seed presents high-indexed or defect surfaces [66]. When the amount of $HAuCl_4$ in the growth solution was kept low (~1.2 mM), among the four structures that were obtained, the

growth in the presence of A10 was unique in that it formed a rough coat of gold over the concave seed, while the other three bases showed very similar morphologies (Fig. S15). The initial growth process is mostly dominated by the seed surface energies to make final morphologies indistinguishable and independent of which base is used in the growth (T10, G10 and C10). A10, however is an exception, due to its high binding affinity to the seed and precursor. The effect of A10-mediated growth is distinctly visible even in the presence of a lower amount of precursor through the formation of the rough particle. Despite the difference, the deposition of Au was more along the edges and vertices of the seed in presence of all the bases. In contrast, the previous study using simple Pd cubic seed showed that the shell deposition was completely site specific on the seed depending on the DNA sequence used. With respect to the other DNA sequences, different morphologies arise only after further reduction of gold. The high γ of the edges and the vertices of the concave seed have more influence on the deposition of gold on to these sites than the sites with lower γ. After the initial deposition of gold on the seed to form a shell, the growth beyond that point can be treated as the formation of the shell on a core with surfaces that now have comparatively lower γ than the naked concave Pd seed. It is known that the affinity of the DNA bases to gold takes the order of A > C ≥ G > T [67] and essentially, the current condition can clearly differentiate between the effect of high binding affinity ligands such as A10 from the effect of low or medium binding affinity DNA (T10, G10 and C10) which is predominant during the later stage of the Au shell growth on the concave seed to form asymmetric structures. Additionally, when we tried a “block” combination sequence such as AAAAACCCCC (A5C5), the morphology was indeed dominated by the A base resulting in a rough growth of the gold shell on the Pd concave nanoparticle, (Figure S16) further suggesting the importance of base affinity.

Furthermore, on studying the absorption spectra of the particles formed by the reduction of lower concentration of $HAuCl_4$ (~1.2 mM), we found that only the λ_{max} value of the absorption spectrum for the A10-mediated particles was unique in comparison to that of T10, G10 and C10-mediated particles, whose spectra were very similar (Fig. S17). It is essential to note that the lower concentration of HAuCl4 is equivalent to the concentration used in the simple cubic system [48]. An important observation is the absence of the shoulder peak in almost all of the spectra. This observation suggests that the anisotropicity of the particles increases on further reduction of $HAuCl_4$ mediated by the DNA. The kinetic study of particle growth in presence of A10 and T10 gave us data that was in agreement with what we observed in the presence of higher $HAuCl_4$ concentration (~3.6 mM). A sigmoidal kinetic curve was observed in presence of A10 and an exponential growth curve was observed in the presence of T10 (Fig. S18).

3.2 Comparison of DNA-mediated growth of Au shell onto cubic core and concave cubic core:

It is well known that metal nanoparticle synthesis involves many interdependent factors that affect the final morphology. Factors such as temperature may also play a role in affecting the kinetic parameters of a DNA-mediated nanoparticle growth [49]. Much higher temperatures than room temperature, investigated in this work, may prevent the interaction of DNA to the metal surface and thus lead to the formation of nanoparticles with less controlled

morphology. While a much lower temperature will reduce the rate of reduction and thus more effective control of morphology, it may restrict the movement or flexibility of the DNA strand. It is hence important to decouple parameters of growth in order to better understand existing nanoparticle growth systems. In a typical seed mediated nanoparticle synthesis, among the key factors that are taken into consideration, the characteristics of the seed are vital [68–70]. Generally, in growth systems that involves hetero phases and high-indexed seeds, the growth of the hetero phase is heavily influenced by the seed due to higher surface energies and often proceeds in a conformal manner [71–74]. A comparison between the simple cubic and the concave cubic core Pd seeds reveal differences in the DNA-mediated growth on Au shell. 1) In the simple cubic seed (SPR ~400 nm), the emergence of the plasmonic peak (due to Au deposition) did not exhibit any shift in the λ_{max}, while the concave cube (SPR ~700nm) showed a shift in λ_{max}, suggesting SPR coupling between the Pd seed and the depositing Au in the latter system, but not the former. The absorption spectra of the simple cubic system has a narrow window that fails to couple with the emerging absorption of the depositing shell around ~ 600 nm. In case of the concave cubic system which has a broad absorption spanning the visible and the NIR range that readily shows plasmonic coupling with the depositing gold; 2) The growth rate is faster using Pd concave cube as the seed (~35 min) than when using the Pd cube as the seed (> 1 h), even though the growth solution contains equal amounts of reductant. It should be noted, however, that decreasing the precursor concentration slowed the reaction down slightly but the overall growth process is consistently faster than the system with the simple cubic core, indicating that the concave seed allows faster nucleation of gold; 3) With the simple cubic core, the influence of DNA was evident from the very beginning of the growth, where the DNA sequences controlled the deposition by surface passivation in a sequence dependent manner; in contrast, the initial growth in the concave cube core is heavily dictated by the seed's surface energy. Despite the differences, the aggregative growth mechanism in the presence of A10 is similar in both systems, in the absorbance vs time kinetic profiles, the rise in absorbance takes place in ~5 min for the concave cube vs the ~10 min in the presence of the simple cube, in agreement with the increased growth rate. These subtle but important differences strongly suggest that the interactions between the DNA molecules and different seeds, that have different properties, play an important role in determining the growth parameters and have substantial influence on the final nanoparticle morphologies.

4 Conclusion

In this study, we have demonstrated that, even in the presence of a seed with high energy-indexed facets like the concave nanocube, DNA can still direct the seed-mediated synthesis of bimetallic nanoparticles, resulting in four architecturally disparate Pd@Au core-shell structures in the presence of 10-mer sequences of adenine, thymine, guanine and cytosine. Based on detailed spectroscopic and SEM studies of time-dependent growth of the bimetallic nanoparticles, we have discovered the following general principles when DNA sequences matter even when the seed contains high-energy facets. 1) Each sequence has a unique way of interacting with both the seed's surface and the precursor, given the disparate chemical functionalities that the DNA bases have. Among them, the most important factor is the binding affinity of the base. A10 for example, has the highest binding affinity and was

capable of stabilizing the seed's high energy surfaces. Hence, A10 still induced an aggregative growth mechanism; 2) For bases with lower or medium binding affinity (T10, G10 and C10), the initial growth is completely dictated by the seed's surface energy. The overall growth process for all the bases proceeds in a manner where the $V_{deposition}$ is always greater than the $V_{diffusion}$; 3) The effect of low or medium binding affinity DNA can be observed after further reduction of metal onto the concave seed i.e. the effect of DNA comes into play after the initial passivation of the low co-ordination, high-energy sites on the seed. Essentially, to obtain disparate core-shell morphologies for a given seed in a DNA-mediated synthesis, the precursor investment for a given DNA concentration and each synthesis changes depending on the seed's characteristics. Overall, this study has provided insights into factors governing growth of core-shell structures using seeds with high-energy indexes, and these insights can readily be applied to other bimetallic systems where DNA is used as a capping ligand.

Supplementary Material

Refer to Web version on PubMed Central for supplementary material.

Acknowledgements

We wish to thank the U.S. National Institutes of Health (GM124316 and MH110975) for financial support. N. S. R. S. would like to thank the Beckman Graduate Fellowship for financial support. The authors thank Prof. Hong Yang, Prof. Kenneth S. Suslick, and Prof. Catherine J. Murphy for their insightful discussions. SEM, TEM, and STEM were carried out at the Federick Seitz Materials Research Laboratory Central Research Facilities, University of Illinois. The authors also thank Dr. Moitree Laskar for suggestions in a synthetic protocol, Dianwen Zhang for help with the confocal Raman microscopy, Kapil Dave for CD measurements, Kevin Harnden for help with data analysis and Vishwas Srivastava for help with HR-TEM and helpful discussions.

References

[1]. Tao AR; Habas S; Yang P, Shape Control of Colloidal Metal Nanocrystals. Small 2008, 4 (3), 310–325.

[2]. Xia Y; Xiong Y; Lim B; Skrabalak SE, Shape-Controlled Synthesis of Metal Nanocrystals: Simple Chemistry Meets Complex Physics? Angew. Chem. Int. Ed 2009, 48 (1), 60–103.

[3]. Tan LH; Xing H; Lu Y, DNA as a Powerful Tool for Morphology Control, Spatial Positioning, and Dynamic Assembly of Nanoparticles. Acc. Chem. Res 2014, 47 (6), 1881–1890. [PubMed: 24871359]

[4]. Xia Y; Xia X; Peng H-C, Shape-Controlled Synthesis of Colloidal Metal Nanocrystals: Thermodynamic versus Kinetic Products. J. Am. Chem. Soc 2015, 137 (25), 7947–7966. [PubMed: 26020837]

[5]. Barnes WL; Dereux A; Ebbesen TW, Surface plasmon subwavelength optics. Nature 2003, 424 (6950), 824–830. [PubMed: 12917696]

[6]. Hutter E; Fendler JH, Exploitation of Localized Surface Plasmon Resonance. Adv. Mater 2004, 16 (19), 1685–1706.

[7]. Murphy CJ; Sau TK; Gole AM; Orendorff CJ; Gao J; Gou L; Hunyadi SE; Li T, Anisotropic Metal Nanopartides: Synthesis, Assembly, and Optical Applications. J. Phys. Chem. B 2005, 109 (29), 13857–13870. [PubMed: 16852739]

[8]. Lal S; Link S; Halas NJ, Nano-optics from sensing to waveguiding. Nat Photon 2007, 1 (11), 641–648.

[9]. Wang F; Han Y; Lim CS; Lu Y; Wang J; Xu J; Chen H; Zhang C; Hong M; Liu X, Simultaneous phase and size control of upconversion nanocrystals through lanthanide doping. Nature 2010, 463 (7284), 1061–1065. [PubMed: 20182508]

[10]. Liu J; Duchesne PN; Yu M; Jiang X; Ning X; Vinluan RD; Zhang P; Zheng J, Luminescent Gold Nanoparticles with Size-Independent Emission. Angew. Chem. Int. Ed 2016, 55 (31), 8894–8898.

[11]. Narayanan R; El-Sayed MA, Catalysis with Transition Metal Nanopartides in Colloidal Solution: Nanoparticle Shape Dependence and Stability. J. Phys. Chem. B 2005, 109 (26), 12663–12676. [PubMed: 16852568]

[12]. Astruc D; Lu F; Aranzaes JR, Nanoparticles as Recyclable Catalysts: The Frontier between Homogeneous and Heterogeneous Catalysis. Angew. Chem. Int. Ed 2005, 44 (48), 7852–7872.

[13]. Wei H; Lu Y, Catalysis of Gold Nanoparticles within Lysozyme Single Crystals. Chemistry - An Asian Journal 2012, 7 (4), 680–683.

[14]. Mahmoud MA; Narayanan R; El-Sayed MA, Enhancing Colloidal Metallic Nanocatalysis: Sharp Edges and Corners for Solid Nanoparticles and Cage Effect for Hollow Ones. Acc. Chem. Res 2013, 46 (8), 1795–1805. [PubMed: 23387515]

[15]. Qian K; Sweeny BC; Johnston-Peck AC; Niu W; Graham JO; DuChene JS; Qiu J; Wang Y-C; Engelhard MH; Su D; Stach E; Wei WD, Surface Plasmon-Driven Water Reduction: Gold Nanoparticle Size Matters. J. Am. Chem. Soc 2014, 136 (28), 9842–9845. [PubMed: 24972055]

[16]. Wei DW; Sweeny CB; Qiu J; DuChene SJ, Metallic Nanostructures for Catalytic Applications In Metallic Nanostructures: From Controlled Synthesis to Applications, Xiong Y; Lu X, Eds. Springer International Publishing: Cham, 2015; pp 243–269.

[17]. Liu J; Lu Y, A Colorimetric Lead Biosensor Using DNAzyme-Directed Assembly of Gold Nanoparticles. J. Am. Chem. Soc 2003, 125 (22), 6642–6643. [PubMed: 12769568]

[18]. Rosi NL; Mirkin CA, Nanostructures in Biodiagnostics. Chem. Rev 2005, 105 (4), 1547–1562. [PubMed: 15826019]

[19]. Lu Y; Liu J, Functional DNA nanotechnology: emerging applications of DNAzymes and aptamers. Curr Opin. Biotechnol 2006, 17 (6), 580–588. [PubMed: 17056247]

[20]. Liu J; Mazumdar D; Lu Y, A Simple and Sensitive “Dipstick” Test in Serum Based on Lateral Flow Separation of Aptamer-Linked Nanostructures. Angew. Chem. Int. Ed 2006, 45 (47), 7955–7959.

[21]. Lee K-S; El-Sayed MA, Gold and Silver Nanoparticles in Sensing and Imaging: Sensitivity of Plasmon Response to Size, Shape, and Metal Composition. J. Phys. Chem. B 2006, 110 (39), 19220–19225. [PubMed: 17004772]

[22]. Huang X; El-Sayed IH; Qian W; El-Sayed MA, Cancer Cell Imaging and Photothermal Therapy in the Near-Infrared Region by Using Gold Nanorods. J. Am. Chem. Soc 2006, 128 (6), 2115–2120. [PubMed: 16464114]

[23]. Wu P; Hwang K; Lan T; Lu Y, A DNAzyme-Gold Nanoparticle Probe for Uranyl Ion in Living Cells. J. Am. Chem. Soc 2013, 135 (14), 5254–5257. [PubMed: 23531046]

[24]. Zhang J; Cheng F; Li J; Zhu J-J; Lu Y, Fluorescent nanoprobes for sensing and imaging of metal ions: Recent advances and future perspectives. Nano Today 2016, 11(3), 309–329. [PubMed: 27818705]

[25]. Smith BR; Gambhir SS, Nanomaterials for In Vivo Imaging. Chem. Rev 2017, 117 (3), 901–986. [PubMed: 28045253]

[26]. Jain PK; Lee KS; El-Sayed IH; El-Sayed MA, Calculated Absorption and Scattering Properties of Gold Nanoparticles of Different Size, Shape, and Composition: Applications in Biological Imaging and Biomedicine. J. Phys. Chem. B 2006, 110 (14), 7238–7248. [PubMed: 16599493]

[27]. Lu Y; Liu J, Smart Nanomaterials Inspired by Biology: Dynamic Assembly of Error-Free Nanomaterials in Response to Multiple Chemical and Biological Stimuli. Acc. Chem. Res 2007, 40 (5), 315–323. [PubMed: 17474707]

[28]. Jain PK; Huang X; El-Sayed IH; El-Sayed MA, Noble Metals on the Nanoscale: Optical and Photothermal Properties and Some Applications in Imaging, Sensing, Biology, and Medicine. Acc. Chem. Res 2008, 41 (12), 1578–1586. [PubMed: 18447366]

[29]. Dreaden EC; Alkilany AM; Huang X; Murphy CJ; El-Sayed MA, The golden age: gold nanoparticles for biomedicine. Chem. Soc. Rev 2012, 41 (7), 2740–2779. [PubMed: 22109657]

[30]. Xing H; Hwang K; Li J; Torabi S-F; Lu Y, DNA aptamer technology for personalized medicine. Current Opinion in Chemical Engineering 2014, 4, 79–87. [PubMed: 24791224]

[31]. Tao Y; Li M; Ren J; Qu X, Metal nanoclusters: novel probes for diagnostic and therapeutic applications. Chem. Soc. Rev 2015, 44 (23), 8636–8663. [PubMed: 26400655]

[32]. Yu M; Zheng J, Clearance Pathways and Tumor Targeting of Imaging Nanoparticles. ACS Nano 2015, 9(7), 6655–6674. [PubMed: 26149184]

[33]. Wang W; Satyavolu NSR; Wu Z; Zhang J-R; Zhu J-J; Lu Y, Near-Infrared Photothermally Activated DNAzyme-Gold Nanoshells for Imaging Metal Ions in Living Cells. Angew. Chem. Int. Ed 2017, 56 (24), 6798–6802.

[34]. DuChene JS; Niu W; Abendroth JM; Sun Q; Zhao W; Huo F; Wei WD, Halide Anions as Shape-Directing Agents for Obtaining High-Quality Anisotropic Gold Nanostructures. Chem. Mater 2013, 25 (8), 1392–1399.

[35]. Ortiz N; Skrabalak SE, On the Dual Roles of Ligands in the Synthesis of Colloidal Metal Nanostructures. Langmuir 2014, 30 (23), 6649–6659. [PubMed: 24446902]

[36]. Mirkin CA; Letsinger RL; Mucic RC; Storhoff JJ, A DNA-based method for rationally assembling nanoparticles into macroscopic materials. Nature 1996, 382 (6592), 607–609. [PubMed: 8757129]

[37]. Zhang F; Nangreave J; Liu Y; Yan H, Structural DNA Nanotechnology: State of the Art and Future Perspective. J. Am. Chem. Soc 2014, 136 (32), 11198–11211. [PubMed: 25029570]

[38]. Torabi S-F; Lu Y, Functional DNA nanomaterials for sensing and imaging in living cells. Curr. Opin. Biotechnol 2014, 28, 88–95. [PubMed: 24468446]

[39]. Li Y; Liu Z; Yu G; Jiang W; Mao C, Self-Assembly of Molecule-like Nanoparticle Clusters Directed by DNA Nanocages. J. Am. Chem. Soc 2015, 137 (13), 4320–4323. [PubMed: 25823595]

[40]. Liu Z; Tian C; Yu J; Li Y; Jiang W; Mao C, Self-Assembly of Responsive Multilayered DNA Nanocages. J. Am. Chem. Soc 2015, 137 (5), 1730–1733. [PubMed: 25628147]

[41]. Veneziano R; Ratanalert S; Zhang K; Zhang F; Yan H; Chiu W; Bathe M, Designer nanoscale DNA assemblies programmed from the top down. Science 2016, 352 (6293), 1534–1534. [PubMed: 27229143]

[42]. Wu X; Xu L; Ma W; Liu L; Kuang H; Kotov NA; Xu C, Propeller-Like Nanorod-Upconversion Nanoparticle Assemblies with Intense Chiroptical Activity and Luminescence Enhancement in Aqueous Phase. Adv. Mater 2016, 28 (28), 5907–5915. [PubMed: 27158947]

[43]. Wang Z; Zhang J; Ekman JM; Kenis PJA; Lu Y, DNA-Mediated Control of Metal Nanoparticle Shape: One-Pot Synthesis and Cellular Uptake of Highly Stable and Functional Gold Nanoflowers. Nano Lett. 2010, 10(5), 1886–1891. [PubMed: 20405820]

[44]. Wang Z; Tang L; Tan LH; Li J; Lu Y, Discovery of the DNA “Genetic Code” for Abiological Gold Nanoparticle Morphologies. Angew. Chem. Int. Ed 2012, 51 (36), 9078–9082.

[45]. Wu J; Tan LH; Hwang K; Xing H; Wu P; Li W; Lu Y, DNA Sequence-Dependent Morphological Evolution of Silver Nanoparticles and Their Optical and Hybridization Properties. J. Am. Chem. Soc 2014, 136 (43), 15195–15202. [PubMed: 25243485]

[46]. Song T; Tang L; Tan LH; Wang X; Satyavolu NSR; Xing H; Wang Z; Li J; Liang H; Lu Y, DNA-Encoded Tuning of Geometric and Plasmonic Properties of Nanoparticles Growing from Gold Nanorod Seeds. Angew. Chem. Int. Ed 2015, 54 (28), 8114–8118.

[47]. Tan LH; Yue Y; Satyavolu NSR; Ali AS; Wang Z; Wu Y; Lu Y, Mechanistic Insight into DNA-Guided Control of Nanoparticle Morphologies. J. Am. Chem. Soc 2015, 137 (45), 14456–14464. [PubMed: 26492515]

[48]. Satyavolu NSR; Tan LH; Lu Y, DNA-Mediated Morphological Control of Pd-Au Bimetallic Nanoparticles. J. Am. Chem. Soc 2016, 138 (50), 16542–16548. [PubMed: 27935691]

[49]. Li J; Zhu Z; Liu F; Zhu B; Ma Y; Yan J; Lin B; Ke G; Liu R; Zhou L; Tu S; Yang C, DNA-Mediated Morphological Control of Silver Nanoparticles. Small 2016, 12 (39), 5449–5487. [PubMed: 27551864]

[50]. Laskar M; Skrabalak SE, Decoupling the Geometric Parameters of Shape-Controlled Pd Nanocatalysts. ACS Catal. 2014, 4 (4), 1120–1128.

[51]. Niu W; Zhang W; Firdoz S; Lu X, Controlled Synthesis of Palladium Concave Nanocubes with Sub-10-Nanometer Edges and Corners for Tunable Plasmonic Property. Chem. Mater 2014, 26 (6), 2180–2186.

[52]. Jin M; Zhang H; Xie Z; Xia Y, Palladium Concave Nanocubes with High-Index Facets and Their Enhanced Catalytic Properties. Angew. Chem. Int. Ed 2011, 50(34), 7850–7854.

[53]. Yu Y; Zhang Q; Xie J; Lee JY, Engineering the architectural diversity of heterogeneous metallic nanocrystals. Nat. Commun 2013, 4, 1454. [PubMed: 23385598]

[54]. Sabir TS; Yan D; Milligan JR; Aruni AW; Nick KE; Ramon RH; Hughes JA; Chen Q; Kurti RS; Perry CC, Kinetics of Gold Nanoparticle Formation Facilitated by Triblock Copolymers. J. Phys. Chem. C 2012, 116 (7), 4431–4441.

[55]. Han L; Maye MM; Leibowitz FL; Ly NK; Zhong C-J, Quartz-crystal microbalance and spectrophotometric assessments of inter-core and inter-shell reactivities in nanoparticle thin film formation and growth. J. Mater. Chem 2001, 11 (4), 1258–1264.

[56]. Richards VN; Rath NP; Buhro WE, Pathway from a Molecular Precursor to Silver Nanoparticles: The Prominent Role of Aggregative Growth. Chem. Mater 2010, 22 (11), 3556–3567.

[57]. Njoki PN; Luo J; Kamundi MM; Lim S; Zhong C-J, Aggregative Growth in the Size-Controlled Growth of Monodispersed Gold Nanoparticles. Langmuir 2010, 26 (16), 13622–13629. [PubMed: 20695612]

[58]. Thanh NTK; Maclean N; Mahiddine S, Mechanisms of Nucleation and Growth of Nanoparticles in Solution. Chem. Rev 2014, 114 (15), 7610–7630. [PubMed: 25003956]

[59]. Harada M; Kizaki S, Formation Mechanism of Gold Nanoparticles Synthesized by Photoreduction in Aqueous Ethanol Solutions of Polymers Using In Situ Quick Scanning X-ray Absorption Fine Structure and Small-Angle X-ray Scattering. Cryst. Growth Des 2016, 16 (3), 1200–1212.

[60]. Zhao L; Ji X; Sun X; Li J; Yang W; Peng X, Formation and Stability of Gold Nanoflowers by the Seeding Approach: The Effect of Intraparticle Ripening. J. Phys. Chem. C 2009, 113 (38), 16645–16651.

[61]. Guozhong CY, Wang, Characterization and Properties of Nanomaterials. In Nanostructures and Nanomaterials, WORLD SCIENTIFIC: 2011; Vol. 2, pp 433–508.

[62]. Chen AN; Scanlan MM; Skrabalak SE, Surface Passivation and Supersaturation: Strategies for Regioselective Deposition in Seeded Syntheses. ACS Nano 2017, 11 (12), 12624–12631. [PubMed: 29164855]

[63]. Xia X; Xie S; Liu M; Peng H-C; Lu N; Wang J; Kim MJ; Xia Y, On the role of surface diffusion in determining the shape or morphology of noble-metal nanocrystals. Proc. Natl. Acad. Sci. U.S.A 2013, 110(17), 6669–6673. [PubMed: 23569268]

[64]. Liu J, Adsorption of DNA onto gold nanoparticles and graphene oxide: surface science and applications. Phys. Chem. Chem. Phys 2012, 14 (30), 10485–10496. [PubMed: 22739570]

[65]. Sanchez-Gaytan BL; Qian Z; Hastings SP; Reca ML; Fakhraai Z; Park S-J, Controlling the Topography and Surface Plasmon Resonance of Gold Nanoshells by a Templated Surfactant-Assisted Seed Growth Method. J. Phys. Chem. C2013, 117 (17), 8916–8923.

[66]. Quan Z; Wang Y; Fang J, High-Index Faceted Noble Metal Nanocrystals. Acc. Chem. Res 2013, 46 (2), 191–202. [PubMed: 22587943]

[67]. Kimura-Suda H; Petrovykh DY; Tarlov MJ; Whitman LJ, Base-dependent competitive adsorption of single-stranded DNA on gold. J. Am. Chem. Soc 2003, 125, 9014. [PubMed: 15369348]

[68]. DeSantis CJ; Skrabalak SE, Core Values: Elucidating the Role of Seed Structure in the Synthesis of Symmetrically Branched Nanocrystals. J. Am. Chem. Soc 2013, 135 (1), 10–13. [PubMed: 23270415]

[69]. Weiner RG; DeSantis CJ; Cardoso MBT; Skrabalak SE, Diffusion and Seed Shape: Intertwined Parameters in the Synthesis of Branched Metal Nanostructures. ACS Nano 2014, 8 (8), 8625–8635. [PubMed: 25133784]

[70]. Xia Y; Gilroy KD; Peng H-C; Xia X, Seed-Mediated Growth of Colloidal Metal Nanocrystals. Angew. Chem. Int. Ed 2017, 56 (1), 60–95.

[71]. Habas SE; Lee H; Radmilovic V; Somorjai GA; Yang P, Shaping binary metal nanocrystals through epitaxial seeded growth. Nat. Mater 2007, 6 (9), 692–697. [PubMed: 17618289]

[72]. Yu Y; Zhang Q; Liu B; Lee JY, Synthesis of Nanocrystals with Variable High-Index Pd Facets through the Controlled Heteroepitaxial Growth of Trisoctahedral Au Templates. J. Am. Chem. Soc 2010, 132 (51), 18258–18265. [PubMed: 21141886]

[73]. Wang F; Li C; Sun L-D; Wu H; Ming T; Wang J; Yu JC; Yan C-H, Heteroepitaxial Growth of High-Index-Faceted Palladium Nanoshells and Their Catalytic Performance. J. Am. Chem. Soc 2011, 133 (4), 1106–1111. [PubMed: 21174411]

[74]. Jin H; Lee KW; Khi NT; An H; Park J; Baik H; Kim J; Yang H; Lee K, Rational Synthesis of Hetero structured M/Pt (M = Ru or Rh) Octahedral Nanoboxes and Octapods and Their Structure-Dependent Electrochemical Activity Toward the Oxygen Evolution Reaction. Small 2015, 11 (35), 4462–4468. [PubMed: 26081525]

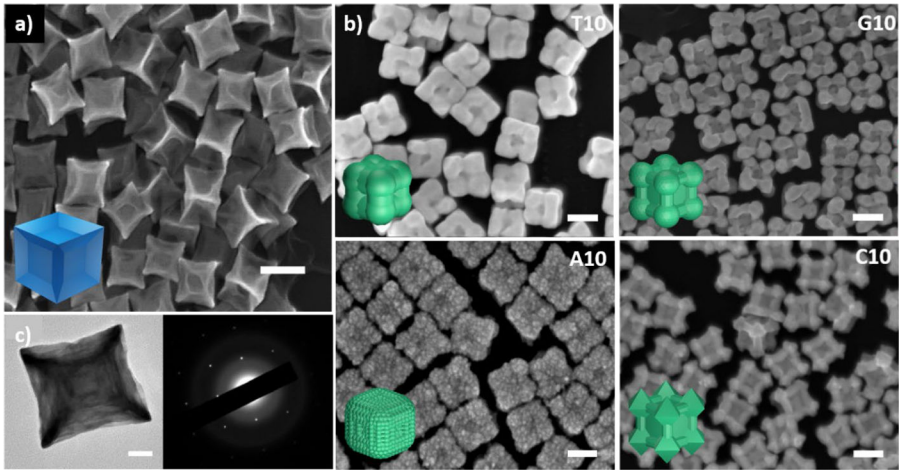

Figure 1.

SEM images of a) Pd concave seed and b) the Pd@Au core-shell nanoparticles synthesized in the presence of DNA molecules (T10, G10, C10 and A10 sequences). Scale bars = 100 nm. Insets represent the schematic representation of the nanoparticle shapes. c) TEM image of the Pd concave seed alongside the SAED (Selected Area Electron Diffraction) of the concave cube implying the retention of the {100} facet at the center. Scale bar = 20 nm.

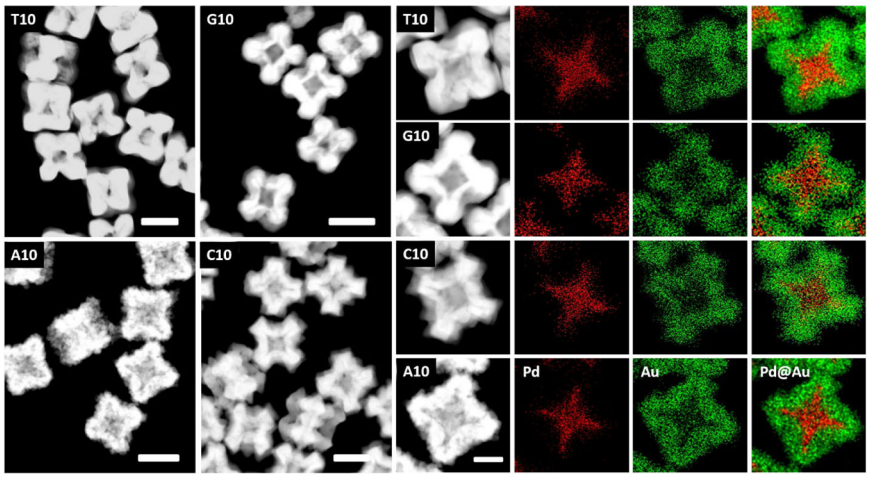

Figure 2.

Left: STEM images of each of the particles. Scale bars 100 nm. Right: Elemental map for each morphology, indicating the composition of the final particles. Scale bar 50 nm.

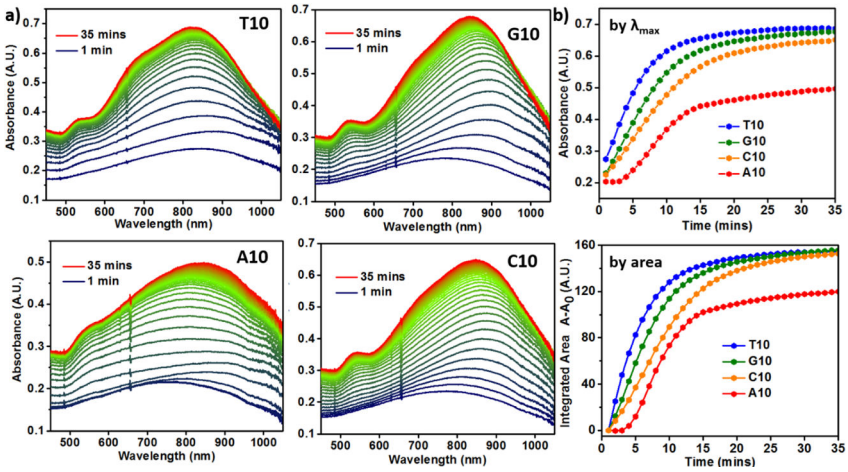

Figure 3.

a) Kinetic absorption spectra of nanoparticle growth in the presence of DNA. b) The plot of absorbance vs time at the λmax values for each morphology (top), the plot of integrated area under the absorption spectra between 500 to 1000 nm vs time for each morphology (bottom).

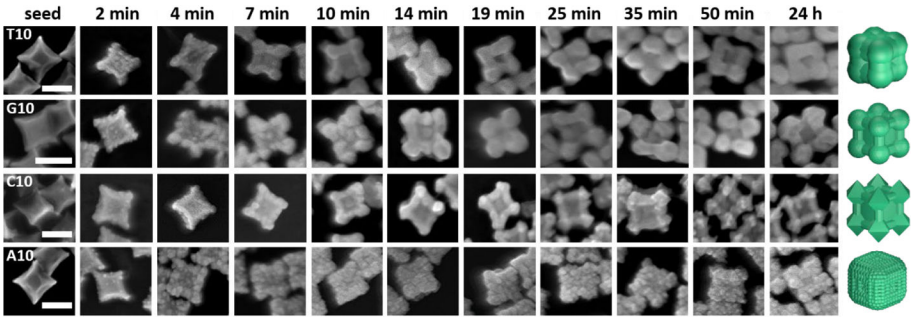

Figure 4.

SEM images of the nanoparticle growth quenched at different time points. Time points were chosen to represent the morphology evolution in the presence of each of the DNA sequence. Scale bars = 100 nm.

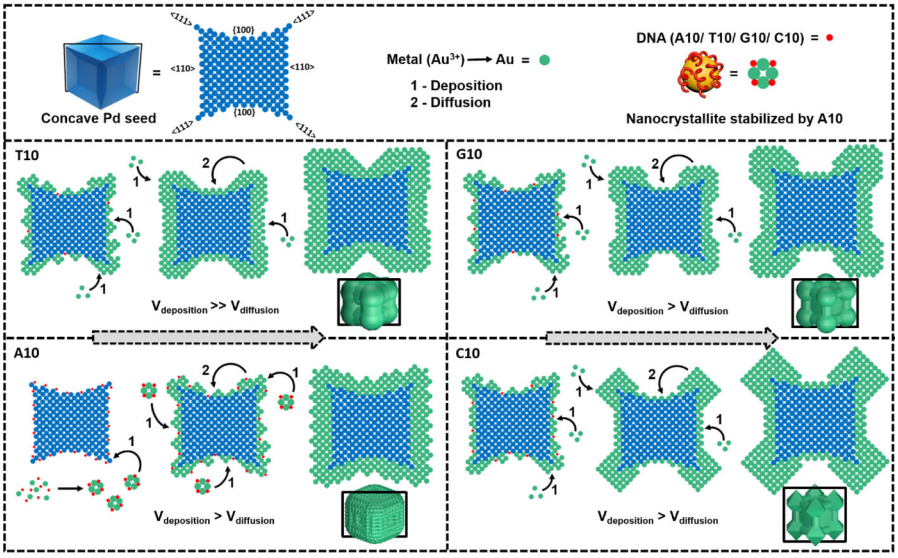

Scheme 1.

Proposed Mechanism of Growth of Pd@Au Core-Shell Nanostructures Influenced by Different Sequences of DNA[a]

[a]The atomic models represent the cross-section of the 3-D models along the black box in each individual case.